Trypanosoma cruzi persisters that survive benznidazole treatment *in vitro* and *in vivo* are in a transient non-replicative state

Shiromani Jayawardhana, Alexander I. Ward[1], Amanda F. Francisco, Michael D. Lewis, Martin C. Taylor, John M. Kelly*, Francisco Olmo.

Department of Infection Biology,
London School of Hygiene and Tropical Medicine,
Keppel Street,
London WC1E 7HT, UK.

[1]Current address: Institute of Immunity and Transplantation,
University College London,
Pond Street,
London NW3 2PP, UK.

*Corresponding author: Department of Infection Biology,
London School of Hygiene and Tropical Medicine,
Keppel Street,
London WC1E 7HT, UK.
Tel: 44-20-7927-2330 Email: john.kelly@lshtm.ac.uk

Short running title: Imaging benznidazole treatment failure in experimental Chagas disease

Abstract

Benznidazole is the front-line drug used to treat infections with *Trypanosoma cruzi*, the causative agent of Chagas disease. However, for reasons that are unknown, treatment failures are common. To assess the nature of parasites that persist after treatment, we first exposed infected mammalian cell monolayers to a benznidazole regimen that reduces the intracellular amastigote population to <1% of the pre-treatment level. Of host cells that remained infected, the vast majority contained only one or two surviving intracellular amastigotes. Analysis, using incorporation of the thymidine analogue EdU, revealed these surviving parasites to be in a transient non-replicative state. Furthermore, treatment with benznidazole led to widespread damage to parasite DNA. When parasites that survived treatment in mice were examined using *in vivo* and *ex vivo* bioluminescence imaging, we found that recrudescence is not due to persistence of parasites in a specific organ or tissue that preferentially protects them from drug activity. Surviving parasites were widely distributed and located in host cells where the vast majority contained only one or two amastigotes. Therefore, infection relapse does not arise from a small number of intact large nests. Rather, persisters are either survivors of intracellular populations where co-located parasites have been killed, or amastigotes in single/low-level infected cells exist in a state where they are less susceptible to benznidazole. Assessment by EdU incorporation revealed that the small number of parasites which persist in mice after treatment are initially non-replicative. A possible explanation could be that triggering of the *T. cruzi* DNA damage response pathway by the activity of benznidazole metabolites results in exit from the cell cycle as parasites attempt DNA repair, and that metabolic changes associated with non-proliferation act to reduce drug susceptibility. Alternatively, a small percentage of the parasite population may pre-exist in this non-replicative state prior to treatment.

Author Summary

Trypanosoma cruzi is the causative agent of Chagas disease, the most important parasitic infection in Latin America. For reasons that are not established, the front-line drug benznidazole often fails to achieve sterile cure. Here, we used highly sensitive imaging technology to investigate the impact of benznidazole on *T. cruzi* infected mice. Following non-curative treatment, we found that persistence is not restricted to a specific organ or tissue that preferentially protects the parasite from drug activity. Rather, surviving parasites are widely distributed, although overall tissue levels are extremely low. These persisters are located in host cells that typically contain only one or two non-replicating intracellular amastigotes. However, these parasites re-initiate DNA replication within several days of treatment cessation and begin to proliferate. Therefore, being in a non-replicative state seems to confer protection against drug-mediated trypanocidal activity. Benznidazole treatment results in widespread damage to parasite DNA. One possibility therefore, is that this triggers the *T. cruzi* DNA damage response pathway, resulting in exit from the cell cycle as parasites attempt DNA repair. Alternatively, persisters may be derived from a small parasite sub-population that pre-exists in a non-replicative state prior to treatment.

Introduction

Chagas disease is caused by the insect-transmitted protozoan parasite *Trypanosoma cruzi* and is a major public health problem throughout Latin America, with 6 - 7 million people infected [1]. In addition, many cases are now being detected within migrant populations world-wide, particularly in Europe and the USA [2,3]. *T. cruzi* is an obligate intracellular parasite, with a wide host cell range. During the acute stage of the disease, which in humans occurs 2 - 8 weeks post-infection, parasites become widely disseminated in blood and tissues, and the infection manifests as a transient, typically mild, febrile condition. In children, the acute stage can be more serious, sometimes resulting in myocarditis or meningoencephalitis, with fatal outcomes in 5% of diagnosed cases. The acute stage is normally controlled by adaptive immune responses, mediated by $CD8^+$ IFN-γ^+ T cells [4], with the infection then advancing to an asymptomatic chronic stage, in which the parasite burden is extremely low and focally restricted. However, 30 - 40% of those that are chronically infected eventually progress to a symptomatic stage, although this can take decades. Most develop cardiomyopathy, or less commonly, digestive tract megasyndromes, or both [5,6]. Infection with *T. cruzi* is a major cause of heart disease throughout endemic regions.

The nitroheterocyclic compound benznidazole is the front-line drug for *T. cruzi* infection [7,8]. Although it has been in use for almost 50 years, treatment failures are common [9-11]. Several factors have been implicated, including the effects of drug toxicity and the long administration period (60 - 90 days) on patient compliance, and the diverse nature of the *T. cruzi* species, which exhibits significant natural variation in drug susceptibility, both within and between lineages [12,13]. In addition, spontaneous parasite dormancy [14], stress-induced cell cycle arrest [15], and a reduced proliferation rate during the chronic stage [16] have all been proposed as potential mechanisms that could protect the parasite from drug treatment. Benznidazole is a pro-drug and must be activated within the parasite by the mitochondrial nitroreductase TcNTR-1 [7,12,17]. Although the precise mode of action remains to be resolved, current evidence supports a mechanism whereby highly mutagenic benznidazole

113 metabolites, including glyoxal, cause widespread damage to genomic DNA [18-20].
114 Furthermore, there is a potential for cross-resistance to the other anti-*T. cruzi* drug nifurtimox,
115 which also requires TcNTR-1-mediated activation [17,21].
116
117 In recent clinical trials, benznidazole treatment failure has been reported in 20-50% of patients
118 [10]. Investigating the reasons for this has been complicated by the extremely low parasite
119 burden, the focal nature of chronic infections, and the resultant difficulties in establishing
120 cure/non-cure. It is unclear, for example, whether *T. cruzi* is able to persist in specific tissues
121 or organs that are less accessible to benznidazole, or if a sub-set of dormant or metabolically
122 quiescent parasites are able to survive drug exposure that kills the majority of the parasite
123 population. To better investigate treatment failure, we have exploited a genetically modified
124 parasite cell line that expresses a reporter fusion protein that is both bioluminescent and
125 fluorescent [22]. The red-shifted bioluminescent component of this protein allows the tissue-
126 specific location of parasites to be resolved with exquisite sensitivity during murine infections
127 [23], and the fluorescent component then enables parasites to be visualized at the level of
128 individual infected cells [24,25]. This has enabled us to localize and characterize parasites
129 that persist after non-curative benznidazole treatment in murine models of acute Chagas
130 disease. Our results indicate that parasites which survive treatment are in a non-replicative
131 state.
132
133
134
135
136
137
138
139
140

141 **Results**

142 ***T. cruzi persisters that survive benznidazole treatment in vitro are in a transient non-***
143 ***replicative state***

144 To generate persisters *in vitro*, we adapted the "washout" protocol described by MacLean *et*
145 *al.* [26], using MA104 cells infected with the *T. cruzi* CL Luc::mNeon clone [22] (Materials and
146 Methods). A treatment period of 8 days and a benznidazole concentration of 20 μM (10x
147 amastigote EC_{50}) was assessed as being optimal for this parasite strain:host-cell type
148 combination (Figure 1). Under these conditions, all parasites stopped replicating within 4 days
149 of treatment initiation (based on incorporation of the thymidine analogue EdU) (Figure 1a and
150 b), and the amastigote population fell to <1% of the pre-treatment level. In addition, by day 5
151 and beyond, the majority of infected cells contained only one intracellular amastigote (Figure
152 1c). When benznidazole was removed, flagellated trypomastigotes did eventually develop and
153 undergo egress, indicating the long-term viability of at least some of the surviving parasites,
154 even after 8 days exposure to 200 μM (Figure 1d).

155

156 We further examined parasite persisters using live sorting of infected MA104 cells. Cultures
157 of highly infected cells (Figure 1b, as example) were treated with 20 μM benznidazole for 8
158 days, as above, and the cells then detached to generate a suspension (Figure 2a and b,
159 Materials and Methods). Aliquots of the suspension were incubated with propidium iodide and
160 separated using an Aria BD Cell Sorter to determine the level of host cell viability within the
161 population. There was a minimal level of cell death (Figure 2b and c). When host cells were
162 separated based on the presence/absence of parasite-expressed green fluorescence, the vast
163 majority (>99%) were found to be fluorescence-negative. The only fluorescence-positive cells
164 detected were at the lowest gating, with each cell containing only 1, 2 or occasionally 3
165 parasites (Figure 2d and e). Subsequent plating of these infected cells confirmed their viability
166 (Figure 2f), with trypomastigote egress detectable after 7-14 days in culture. Collectively, these
167 experiments indicate that persister parasites that survive benznidazole treatment must either
168 originate from infected host cells in which other co-habiting parasites have been eliminated,

169 despite being exposed to equivalent drug pressure, or there is an intrinsic feature of
170 amastigotes in single/low-level infected cells that can confer protection against benznidazole.
171
172 To assess the replicative status of intracellular amastigotes that persist after 8 days
173 benznidazole exposure, we monitored the incorporation of EdU into parasite DNA (Figure 3).
174 At selected time points post-treatment, cell monolayers were exposed to EdU for 6 hours,
175 coverslips were removed from the 24-well plates, processed (Materials and Methods), and
176 then scanned exhaustively to locate surviving parasites (green fluorescence). The vast
177 majority of the remaining infected cells contained only 1 or 2 amastigotes (Figure 3a).
178 Parasites were then further assessed to identify those that were in S-phase during the 6 hour
179 EdU exposure period (indicated by red fluorescence). In the case of non-treated infected cells,
180 30-50% of intracellular amastigotes are EdU+ve under these conditions, indicative of DNA
181 replication (Figure 1a and 3c). In contrast, of 607 intracellular amastigotes that were detected
182 in the 9 days following cessation of drug treatment, 99.5% were EdU-ve (Figure 3d and e).
183 However, by day 11 some surviving parasites had re-entered the cell cycle as evidenced by
184 increased intracellular numbers and EdU positivity (Figure 3a and e). Therefore, *T. cruzi*
185 amastigotes that persist after benznidazole treatment *in vitro* are in a non-replicative state, but
186 retain a proliferative capacity.
187
188 The bioactivation of benznidazole is initiated by the parasite-specific nitroreductase TcNTR-1,
189 leading to the generation of reactive metabolites that have mutagenic properties [7,12,17-20].
190 A possible outcome of this could be induction of the DNA damage response system in *T. cruzi*,
191 resulting in exit from the cell cycle and entry into a non-proliferative state [27-30]. To
192 investigate the impact of benznidazole on the structural integrity of parasite genomic DNA, we
193 used the TUNEL (terminal deoxynucleotidyl transferase dUTP nick end labelling) assay
194 (Figure 4), a procedure originally developed to monitor apoptotic cell death [31]. In *T. cruzi*,
195 this technique can be used to identify parasites undergoing replication of mitochondrial DNA
196 (kDNA) [22,24]. Parasites early in kDNA S-phase exhibit TUNEL positivity in antipodal sites,

197 either side of the kDNA disk, indicative of the two replication factories (see inset Figure 4b).
198 Later in the cycle, the whole disk becomes labelled. Under normal growth conditions however,
199 *T. cruzi* nuclear DNA does not display a detectable positive signal using this technique. As
200 inferred from TUNEL labelling of free 3'-hydroxyl groups, 24 hours benznidazole treatment
201 (200 μM) resulted in widespread fragmentation of parasite DNA, while the nuclei of adjacent
202 mammalian cells remained unlabelled (Figure 4b). Under these conditions, an 8-fold extension
203 of the treatment period is insufficient to completely eliminate parasites from infected cultures
204 (Figure 1d). As a control, incubation with the hydroperoxide TBHP, which induces apoptosis
205 and necroptosis [32], resulted in lesions to DNA in both parasite and host cells, with a labelling
206 profile similar to that generated by post-fixation DNase treatment (Figure 4b). Thus, DNA
207 damage resulting from benznidazole treatment is parasite-specific, reflecting selective
208 metabolic reduction of the drug by TcNTR-1.
209
210 ***Tissue-specific survival of T. cruzi following benznidazole treatment***
211 Mice in the pre-peak (day 9) and peak phases (day 14) of acute stage infections with the
212 bioluminescent:fluorescent *T. cruzi* reporter strain CL-Luc::Neon [22] were treated once daily
213 for 5 days with benznidazole at 25 mg/kg, a treatment regimen we had previously shown to
214 be non-curative [33]. This resulted in a 97-99% knock-down in the whole-body parasite burden
215 by the end of the treatment period, as inferred by *in vivo* bioluminescence imaging (Figure 5a).
216 *Ex vivo* imaging was then used to examine organs and tissues. In non-treated mice, the
217 infection was widely disseminated, with all organs and tissues highly bioluminescent (Figure
218 5b and c). Drug treatment resulted in a major reduction in both the parasite load and the
219 number of infection sites, although complete parasite clearance was not observed.
220 Importantly, there was no indication from the pattern of the remaining bioluminescent foci that
221 any specific tissue or organ had acted as a location where parasites were preferentially
222 protected from drug activity (Figure 5c). This is consistent with benznidazole pharmacokinetics
223 in *T. cruzi* infected mice, where there is extensive bio-distribution of the drug amongst organs
224 and tissues [34].

225

226 Tissue samples containing bioluminescent foci were excised and examined by confocal laser
227 scanning microscopy (Materials and Methods). mNeonGreen fluorescence was detectable in
228 all tissue samples obtained from infected non-treated mice in the pre-peak and peak phases
229 of the acute stage, and parasite location could be established at single-cell resolution [25]
230 (Figure 5d). In infected host cells, parasite numbers were then determined with precision using
231 serial z-stacking (Figure 6a). Tissues examined included the heart, adipose tissue, bladder,
232 spleen, peritoneum, lungs, liver, colon, rectum, cecum, stomach and skeletal muscle.
233 Intracellular amastigote numbers varied considerably in non-treated mice. The vast majority
234 of infected cells had a burden of less than 50 parasites, although occasional large "nests" that
235 contained up to 150 parasites could be detected (1.5% of infected cells) (Figure 6b). Tissue
236 and organs from benznidazole-treated mice were similarly processed on the day following
237 treatment cessation. Infected cells were much less abundant, and were more difficult to locate.
238 Across a range of tissue types, the majority of infected cells (>75%) contained only a single
239 amastigote (Figure 6b). It is implicit therefore, that recrudescence after drug treatment does
240 not arise from the survival of a small number of intact large nests. As with the situation *in vitro*,
241 the most parsimonious explanation is that persisters are the survivors from intracellular
242 populations where the other parasites have been killed. Alternatively, amastigotes in
243 single/low-level infected cells may exist in a state where they are less susceptible to the
244 trypanocidal activity of benznidazole. Treatment at higher doses (100 mg/kg, 5 days), or for
245 longer periods (30 mg/kg, 10 days), also results in relapse (S1 Figure). However, immediately
246 after treatment cessation with these regimens, it is more technically challenging to detect the
247 small number of surviving tissue-resident parasites.

248

249 **Parasites that survive benznidazole treatment *in vivo* are in a non-replicative state.**

250 As above, BALB/c mice in the acute stage of infection were treated with a non-curative
251 benznidazole dosing regimen (5 days, 25 mg/kg). Our strategy was then to use EdU
252 incorporation into parasite DNA as a reporter [16,24], to determine the replicative status of

253 intracellular amastigote persisters (Materials and Methods). However, at this point in the
254 infection (day 20), many of the detected parasites displayed an irregular and diffuse
255 morphology, in both treated and non-treated mice (S2a Figure, as example). In non-treated
256 mice, this was associated with enhanced accumulation of proliferating host cells within
257 infected cardiac tissue (cardiomyocytes are normally terminally differentiated) and a major
258 increase in leukocyte infiltration (S2b Figure). We inferred from this that the observed parasite
259 damage was mediated by the adaptive immune response. To avoid this confounding factor,
260 which would complicate interpretation of the EdU incorporation data, we therefore switched
261 murine models and used CB17 SCID mice, an immunodeficient strain that lacks functional
262 lymphocytes [35]. This resolved the issue, and few proliferating cells were then observed in
263 the cardiac sections (see Figure 7c, for one such example). At the analysis time-point, infected
264 cardiac cells in untreated mice could be readily detected, with the vast majority containing
265 between 1 and 50 morphologically intact parasites. Of the amastigotes surveyed, 45%
266 (845/1863) were found to be in a replicative state as inferred from EdU incorporation (Figure
267 7a and b, S3 Figure, S1 Video). In benznidazole treated CB17 SCID mice, infected cardiac
268 cells were much rarer, with a total of 23 infected cells detected after exhaustive searching of
269 tissue sections. The majority of these contained only a single amastigote (74%, 17/23), and
270 no host cells were found that contained more than 3 parasites (S3 Figure). None of the 30
271 persisting parasites detected in cardiac tissue after benznidazole treatment were in a
272 replicative state, as judged by a lack of incorporation of EdU into genomic and/or kinetoplast
273 DNA (Figure 7a and c, S2 and S3 Videos).
274
275
276
277
278
279
280

281 **Discussion**

282 Benznidazole remains the front-line drug used to treat *T. cruzi* infections, despite multiple
283 reports of treatment failure [9-11]. The underlying reasons for these non-curative outcomes
284 have not been resolved. There is wide diversity in the levels of benznidazole sensitivity within
285 natural *T. cruzi* populations [36]. However, this is not associated with polymorphisms in
286 *TcNTR-1*, the gene that encodes the nitroreductase that initiates reductive activation of the
287 drug [12]. Furthermore, inactivation of one *TcNTR-1* allele results in only a 2 to 4-fold increase
288 in resistance [17], a level insufficient to account for the wide spectrum of benznidazole
289 tolerance within natural populations (~20-fold). Functional disruption of both *TcNTR-1* alleles
290 confers ~10-fold resistance, but this is associated with reduced infectivity that would prevent
291 these highly-resistant parasites from becoming established within host populations [12,17].
292 Other mechanisms must therefore be involved [21].

293

294 In this study, we demonstrate that parasites which survive benznidazole treatment are not
295 preferentially restricted to a specific organ or tissue in experimental mice (Figure 5c). This
296 suggests that variable drug distribution is unlikely to be a major factor in recrudescence, at
297 least in this context. This is in line with studies on benznidazole pharmacokinetics [34]. As an
298 alternative explanation, it has been proposed that the replicative state of intracellular
299 amastigotes could impact on drug sensitivity and that this might have a role in parasite
300 persistence. This follows on from descriptions of apparent dormant forms of the parasite
301 [14,37,38], stress-induced quiescence [15], and a reduced proliferation rate as an adaptation
302 to chronic infection [16]. Here, we found that the small number of amastigotes that survive
303 benznidazole treatment *in vitro* are in a non-replicative state (Figure 3). These persisters
304 remain viable (Figure 2c), and at a population level, retain a capacity to replicate, differentiate
305 and egress from host cells, even after 8 days exposure to 200 μM benznidazole (~100x EC_{50})
306 (Figure 1d). Within 9-11 days of treatment cessation, non-replicative parasites re-enter the
307 cell cycle and to begin to proliferate (Figure 3).

308

309 Are these persister parasites derived from a pre-existing non-replicative sub-population, or do
310 they enter this state as a response to some aspect of drug activity? In the case of
311 benznidazole, damage to parasite DNA is a known mode of action [19,20,39-41]. Reductive
312 drug metabolism is initiated by TcNTR-1, resulting in the production of reactive metabolites
313 that ultimately break down to yield glyoxal [18,42]. These reactive molecules promote the
314 formation of DNA crosslinks, mutagenesis, and chromosomal breaks. In addition, increased
315 oxidative stress gives rise to the formation of oxidized nucleotides, such as 8-oxo-guanine. As
316 further evidence for this mode of action, here we show that benznidazole treatment leads to
317 the generation of extensive parasite-specific DNA breaks detectable by TUNEL assays
318 (Figure 4). An inevitable consequence of this will be induction of the DNA damage response
319 pathway [43], exit from the cell cycle, and recruitment and assembly of DNA repair enzymes
320 at the sites of damage. Lesion repair, if successful, would then be followed by re-entry into the
321 cell cycle and continued proliferation. Therefore, triggering of the *T. cruzi* repair pathways
322 [44,45] by benznidazole may have the effect of inducing a transient non-replicative state that
323 protects at least some parasites from further drug-mediated damage. This does not exclude
324 mechanisms such spontaneous dormancy [14] or other forms of stress-induced quiescence
325 [15] that could act in parallel, or in the case of drugs with a different mode of action, play a key
326 role in persistence.
327
328 When the impact of benznidazole on murine infections was assessed, as with the situation *in*
329 *vitro*, the few parasites that survived treatment were restricted mainly to host cells that
330 contained only one or two amastigotes. This was the case across a wide range of tissue types
331 (Figure 6 and 7), indicating that these scarce residual parasites are the likely source of
332 recrudescence. To assess the replicative status of persisting amastigotes, we focused on
333 cardiac tissue. The heart is the major site of pathology during both the acute (myocarditis) and
334 chronic (cardiomyopathy) stages of Chagas disease. Results from the *in vivo* experiments
335 closely mirrored those from *in vitro* studies. In non-treated mice, maximum nest size was
336 typically up to 50 amastigotes, with 40-50% of the parasite population in S-phase (Figure 7a

337 and b). In contrast, following treatment, nest size was much reduced (typically 1-2 parasites),
338 and all detected parasites were non-replicative (Figure 7a and c, S2 and S3 Videos).
339
340 Remarkably, some parasites that are exposed to continuous benznidazole concentrations of
341 100xEC_{50} for 8 days *in vitro* are able to survive and proliferate (Fig. 1d). *In vivo*, drug exposure
342 following a single dose (25 mg/kg) is considerably less than this, and plasma concentrations
343 drop below the EC_{50} value within 12 hours of administration [33]. Nevertheless, as we show
344 here, 5 days treatment of experimental mice at this dosing regimen is sufficient to kill the vast
345 majority of parasites (Figure 5), with rare non-replicative amastigotes being the only survivors.
346 Attempts to enhance benznidazole efficacy by modifying the dosing regimen have yielded
347 differing results. In murine models, extended intermittent treatment (4 months, twice weekly
348 administration) at 250 mg/kg yielded the best curative outcomes [46]. In contrast, with humans,
349 the cure rate (~80%) using the standard dose remained the same, irrespective of treatment
350 length (once daily for 2 or 8 weeks) [47]. Benznidazole treatment protocols that overcome the
351 problem of persister parasites may be possible, but extended regimens are likely to risk
352 unacceptable toxicity, with a concomitant impact on patient compliance. Combination therapy
353 could be one route to reducing treatment length and benznidazole dose, but clinical trials
354 involving co-treatment with ergosterol biosynthesis inhibitors have shown little benefit [11,47].
355 New anti-*T. cruzi* drugs, delivered individually or in combination will require an ability to
356 eliminate persisters. The recent report that cyanotriazoles can cure experimental infections
357 through selective irreversible binding to topoisomerase II [48] highlights that covalent inhibition
358 of essential enzymes could be one route to achieving parasite elimination.
359
360
361
362
363
364

365 **Materials and Methods**

366 ***In vitro parasite culturing***

367 *T. cruzi* (CL Brener strain) that constitutively express a bioluminescent:fluorescent fusion
368 protein (clone CL-Luc::Neon) were generated and cultured as described previously [22].
369 Metacyclic trypomastigotes were produced by transfer of epimastigotes to Graces-IH medium
370 and harvested after 4-7 days. Tissue culture trypomastigotes (TCTs) were generated after
371 infecting MA104 cells (an African green monkey kidney epithelial cell line) with metacyclic
372 trypomastigotes [16].

373

374 ***Sorting of benznidazole-treated T. cruzi infected cells***

375 T25 tissue culture flasks were seeded with 10^6 MA104 cells, incubated for 6 hours to allow
376 attachment, and then infected with TCTs at an MOI of 10:1 (parasite:host cell). 18 hours later,
377 external parasites were removed by thorough washing (×3), fresh supplemented Minimum
378 Essential Medium Eagle (MEM, Sigma-Aldrich) was added, and benznidazole (Epichem Ltd.)
379 made to a final concentration of 20 μM. The plates were incubated at 37°C, with fresh
380 medium/benznidazole renewed on day 4. After 8 days, the cultures were washed (x2) and
381 cells detached by incubation of the monolayers in TrypLE express (Thermo Fisher). For
382 staining nuclei of live cells, monolayers were incubated with Hoechst 3342 (200 ng/ml) for 90
383 minutes prior to detachment. To differentiate viable/non-viable cells, cellular suspensions were
384 incubated with propidium iodide (PI) (1 μg/ml) for 30 minutes. Following staining and
385 fractionation, the cell suspension was sorted under CL3 conditions using an Aria BD Cell
386 Sorter, with the laser setting appropriate for the stained/fluorescent infected cells.

387

388 ***TUNEL assays***

389 Mammalian cell cultures infected with *T. cruzi* were grown on coverslips in 24-well plates as
390 described above. At specific time points, monolayers were fixed with 4% paraformaldehyde in
391 PBS, air-dried, washed (x1) in PBS, permeabilized in 0.1% TritonX-100/PBS for 5 minutes,
392 and washed (x3) with PBS. 20 μl TUNEL reaction mixture (*In situ* Cell Death Detection Kit,

393 TMR-red, Roche) was then added to each coverslip and the reaction incubated in the dark for
394 1 hour at 37°C. The coverslips were washed (x3) in PBS, mounted on slides with
395 VECTASHIELD® with DAPI (Vector Laboratories, Inc.), and then examined using Zeiss
396 LSM880 confocal or inverted Nikon Ti-2 E inverted microscopes.
397
398 ***In vitro labelling with EdU***
399 As a marker for DNA replication, infected cells were labelled with 5-ethynyl-2′-deoxyuridine
400 (EdU). At various time points after the cessation of benznidazole treatment, fresh medium
401 containing 10 μM EdU (Sigma-Aldrich) was added to selected wells [16] and cultures
402 incubated for a further 6 hours. Monolayers were then washed (x2) and incubated for 45
403 minutes in 4% paraformaldehyde diluted in PBS. Finally, coverslips were removed and
404 washed in PBS (x2). The extent of EdU incorporation was determined using a Click-iT
405 PlusEdU AlexaFluor 555 Imaging kit (Invitrogen), followed by washing with PBS (x2), and the
406 coverslips then mounted in VECTASHIELD® with DAPI. Cells were imaged in three
407 dimensions with a Zeiss LSM880 confocal microscope.
408
409 ***Ethics statement***
410 Animal work was performed under UK Home Office project licences (PPL 70/8207 and PPL
411 P9AEE04E4) and approved by the LSHTM Animal Welfare and Ethical Review Board.
412 Procedures were performed in accordance with the UK Animals (Scientific Procedures) Act
413 1986.
414
415 ***Murine infections***
416 CB17 SCID mice and BALB/c mice were purchased from Charles River (UK). Animals were
417 maintained under specific pathogen-free conditions in individually ventilated cages, with a 12
418 hour light/dark cycle, and access to food and water *ad libitum*. Female CB17 SCID mice, aged
419 9 weeks, were infected with $1x10^3$ TCTs in 0.2 ml 10% fetal calf serum in Dulbecco Minimal
420 Essential Medium (DMEM), with 4.5g/litre glucose, via i.p. injection. BALB/c female mice, aged

421 7-8 weeks, were infected by i.p. injection of $1x10^3$ BTs derived from CB17 SCID mouse blood.
422 At experimental end-points, mice were culled by exsanguination under terminal anaesthesia.
423
424 For drug treatment, benznidazole was prepared for administration at 2.5 or 10 mg/ml in 5%
425 dimethyl sulfoxide (v/v)/95% HPMC suspension vehicle (0.5% (w/v) hydroxypropyl
426 methylcellulose, 0.5% (v/v) benzyl alcohol, 0.4% (v/v) Tween 80 in Milli-Q water). Mice were
427 treated under the regimens outlined in the legends to the relevant figures, with the drug
428 administered by oral gavage [33]. Non-treated control mice were administered with 0.2 ml 5%
429 dimethyl sulfoxide (v/v)/95% HPMC suspension vehicle.
430
431 ***Bioluminescence imaging***
432 Infected mice were injected with 150 mg/kg d-luciferin i.p., then anaesthetized using 2.5% (v/v)
433 gaseous isoflurane 5-10 minutes after d-luciferin administration [49,50]. They were then
434 placed in an IVIS Lumina II Spectrum system (PerkinElmer) and ventral and dorsal images
435 acquired using Living Image v4.7.3. Exposure times varied between 30 seconds and 5
436 minutes, depending on the signal intensity, and anaesthesia was maintained throughout via
437 individual nose cones. For *ex vivo* imaging, mice were injected with d-luciferin, and euthanised
438 as above, then perfused via the heart with 10 ml 0.3 mg/ml d-luciferin in PBS. Organs and
439 tissues were removed and transferred to a Petri dish in a standardized arrangement, soaked
440 in 0.3 mg/ml d-luciferin in PBS, and imaged using maximum detection settings (5 minutes
441 exposure, large binning). The remaining animal parts and carcass were checked for residual
442 bioluminescent foci, also using maximum detection settings. The detection threshold for *in*
443 *vivo* imaging was determined using uninfected mice.
444
445 ***Histological procedures***
446 To ensure preservation of fluorescence in tissue samples derived from infected mice, we
447 adapted methodology previously described [51]. Bioluminescent foci identified by *ex vivo*
448 imaging were excised from tissue and fixed in pre-chilled 95% ethanol for 20-24 hours at 4^oC

449 in histology cassettes. Samples were dehydrated (4x15 minute washes with 100% ethanol),
450 cleared (2x12 minute washes with xylene) and embedded in paraffin wax. Tissue sections (3-
451 10 μM) were cut with a microtome. For confocal imaging, slides were melted on a heat pad
452 for 30 minutes, further de-paraffinized with two changes (12 minutes each) of xylene, three
453 changes (12 minutes each) of Tris-buffered saline, pH 7.6 (TBS), permeabilised with 0.1%
454 Triton X-100 + 0.1% sodium citrate, and then mounted using VECTASHIELD® with DAPI,
455 before storing at 4°C in the dark until required. For immunostaining, slides were blocked and
456 stained with a 1:250 dilution of rat anti-mouse CD45 primary antibody (Tonbo Biosciences;
457 clone 30-F11, cat. #70-0451-U100), used in combination with a 1:500 secondary Alexa Fluor
458 647 donkey anti-rat antibody (Invitrogen Thermo Fisher Scientific, cat. #A-21209).
459

460 ***Confocal and wide-field fluorescence microscopy***

461 For imaging, we used a Zeiss LSM880 confocal laser scanning microscope, with the Zen black
462 software. Accurate determination of intracellular parasite numbers was carried out by 3-
463 dimensional imaging (z-stacking), with the appropriate scan zoom setting [25]. Mounted slides
464 were also imaged using a Nikon Ti-2 E inverted microscope, with images processed using
465 Zen blue software for analysis. Samples were imaged using a Plan Apo 60x oil immersion
466 objective (NA = 1.42, Ph2, Nikon) and an ORCA Flash 4.0 CMOS camera (Hamamatsu). For
467 each specimen, parasites were detected using the green fluorescent channel. In regions of
468 interest, a z-stack of 30 to 50 images with an axial spacing of 0.3 μm was taken for a series
469 of fields of view along the length of the tissue to account for the 3D location of the parasite
470 within individual cells. 3D-video projections were acquired and processed using the NIS
471 Advanced Research software package.
472

473 ***In vivo labelling with EdU***

474 To identify host cells and parasites undergoing DNA replication, mice were given 2 EdU i.p.
475 injections (12.5 mg/kg, 6 hours apart) in PBS at the specific time points as detailed in the
476 Results section. The mice were then left overnight, euthanised by terminal anaesthesia, and

tissue sections fixed and sectioned as above. Labelling of incorporated EdU was carried out using the Click-iT Plus EdU AlexaFluor 555 Imaging kit as described for cultured monolayers.

Acknowledgements

This work was supported by UK Medical Research Council (MRC) grants MR/T015969/1 to J.M.K. and MR/R021430/1 to M.D.L., and funding from the Drugs for Neglected Diseases initiative (DNDi). DNDi received financial support from: Department for International Development (DFID), UK; Federal Ministry of Education and Research (BMBF) through KfW, Germany; and Médecins sans Frontières (MSF) International. AIW was in receipt of an MRC LID (DTP) Studentship (MR/N013638/1).

The funders had no role in study design, data collection and analysis, decision to publish, or preparation of the manuscript.

505 **References**

506 **1.** WHO. *Chagas disease (American trypanosomiasis).* 2018. http://www.who.int/news-
507 room/fact-sheets/detail/chagas-disease-(american-trypanosomiasis).

508 **2.** Bern C, Kjos S, Yabsley MJ, Montgomery SP. *Trypanosoma cruzi* and Chagas'
509 disease in the United States. Clin Microbiol Rev. 2011; 24: 655-681.

510 **3.** Requena-Méndez A, Aldasoro E, de Lazzari E, Sicuri E, Brown M, Moore DA, et al.
511 Prevalence of Chagas disease in Latin-American migrants living in Europe: a
512 systematic review and meta-analysis. PLoS Negl Trop Dis. 2015; 9: e0003540.

513 **4.** Tarleton RL. CD8+ T cells in *Trypanosoma cruzi* infection. Semin Immunopath. 2015;
514 37: 233-238.

515 **5.** Ribeiro AL, Nunes MP, Teixeira MM, Rocha MO. Diagnosis and management of
516 Chagas disease and cardiomyopathy. Nat Rev Cardiol. 2012; 9: 576-589.

517 **6.** Cunha-Neto E, Chevillard C. Chagas disease cardiomyopathy: immunopathology and
518 genetics. Mediat Inflamm. 2014; 2014: 683230.

519 **7.** Wilkinson SR, Kelly JM. Trypanocidal drugs: mechanisms, resistance and new targets.
520 Exp Rev Molec Med. 2009; 11: e31, pp1-24.

521 **8.** Gaspar L, Moraes CB, Freitas-Junior LH, Ferrari S, Costantino L, Costi MP**,** et al.
522 Current and future chemotherapy for Chagas disease. Curr Med Chem. 2015;
523 22:4293-4312.

524 **9.** Molina I, Gómez i Prat J, Salvador F, Treviño B, Sulleiro E, Serre N, et al. Randomized
525 trial of posaconazole and benznidazole for chronic Chagas disease. N Eng J Med.
526 2014; 370: 1899-1908.

527 **10.** Morillo CA, Marin-Neto JA, Avezum A, Sosa-Estani S, Rassi A Jr, Rosas F, et al.
528 Randomized trial of benznidazole for chronic Chagas' cardiomyopathy. N Eng J Med.
529 2015; 373: 1295-1306.

530 **11.** Morillo CA, Waskin H, Sosa-Estani S, Del Carmen Bangher M, Cuneo C, Milesi R, et
531 al. Benznidazole and posaconazole in eliminating parasites in asymptomatic *T. cruzi*
532 carriers: The STOP-CHAGAS trial. J Amer Coll Cardiol. 2017; 69: 939-947.

533 **12.** Mejia AM, Hall BS, Taylor MC, Gómez-Palacio A, Wilkinson SR, Triana-Chávez O, et
534 al. Benznidazole-resistance in *Trypanosoma cruzi* is a readily acquired trait that can
535 arise independently in a single population. J Inf Dis. 2012; 206: 220-228.
536 **13.** Francisco AF, Jayawardhana S, Lewis MD, Taylor MC, Kelly JM. Biological factors that
537 impinge on Chagas disease drug development. Parasitol. 2017; 144: 1871-1880.
538 **14.** Sánchez-Valdéz FJ, Padilla A, Wang W, Orr D, Tarleton RL. Spontaneous dormancy
539 protects *Trypanosoma cruzi* during extended drug exposure. eLife. 2018; 7: e34039.
540 **15.** Dumoulin PC, Burleigh BA. Stress-induced proliferation and cell cycle plasticity of
541 intracellular *Trypanosoma cruzi* amastigotes. mBio. 2018; 9: e00673-18.
542 **16.** Ward AI, Olmo F, Atherton R, Taylor MC, Kelly JM. *Trypanosoma cruzi* amastigotes
543 that persist in the colon during chronic stage murine infections have a reduced
544 replication rate. Open Biology. 2020; 10: 200261.
545 **17.** Wilkinson SR, Taylor MC, Horn D, Kelly JM, Cheeseman I. A mechanism for cross-
546 resistance to nifurtimox and benznidazole in trypanosomes. Proc Natl Acad Sci USA.
547 2008; 105: 5022-5027.
548 **18.** Hall BS, Wilkinson SR. Activation of benznidazole by trypanosomal type I
549 nitroreductases results in glyoxal formation. Antimicrob Agents Chemother. 2012;
550 56: 115-123.
551 **19.** Rajão MA, Furtado C, Alves CL, Passos-Silva DG, de Moura MB, Schamber-Reis BL.
552 Unveiling benznidazole's mechanism of action through overexpression of DNA repair
553 proteins in *Trypanosoma cruzi*. Environ Molec Mutagen. 2014; 55: 309-321.
554 **20.** Campos MC, Phelan J, Francisco AF, Taylor MC, Lewis MD, Pain A, et al. Genome-
555 wide mutagenesis and multi-drug resistance in American trypanosomes induced by
556 the front-line drug benznidazole. Sci Rep. 2017; 7: 14407.
557 **21.** Campos MC, Leon LL, Taylor MC, Kelly JM. Benznidazole-resistance in *Trypanosoma*
558 *cruzi*: evidence that distinct mechanisms can act in concert. Molec Biochem Parasitol.
559 2014; 193: 17-19.

560 **22.** Costa FC, Francisco AF, Jayawardhana S, Calderano SG, Lewis MD, Olmo F, et al.
561 Expanding the toolbox for *Trypanosoma cruzi*: A parasite line incorporating a
562 bioluminescence-fluorescence dual reporter and streamlined CRISPR/Cas9
563 functionality for rapid *in vivo* localisation and phenotyping. PLoS Negl Trop Dis. 2018;
564 12: e0006388.
565 **23.** Lewis MD, Fortes Francisco A, Taylor MC, Burrell-Saward H, McLatchie AP, Miles MA,
566 et al. Bioluminescence imaging of chronic *Trypanosoma cruzi* infections reveals tissue-
567 specific parasite dynamics and heart disease in the absence of locally persistent
568 infection. Cell Microbiol. 2014; 16: 1285-1300.
569 **24.** Taylor MC, Ward A, Olmo F, Jayawardhana S, Francisco AF, Lewis MD, et al.
570 Intracellular DNA replication and differentiation of *Trypanosoma cruzi* is asynchronous
571 within individual host cells *in vivo* at all stages of infection. PLoS Negl Trop Dis. 2020;
572 14: e0008007.
573 **25.** Ward AI, Lewis MD, Khan AA, McCann CJ, Francisco AF, Jayawardhana S, et al. *In*
574 *vivo* analysis of *Trypanosoma cruzi* persistence foci at single cell resolution. mBio.
575 2020; 11: e01242-20.
576 **26.** MacLean LM, Thomas J, Lewis MD, Cotillo I, Gray DW, De Rycker M. Development of
577 *Trypanosoma cruzi in vitro* assays to identify compounds suitable for progression in
578 Chagas' disease drug discovery. PLoS Negl Trop Dis. 2018; 12: e0006612.
579 **27.** Giglia-Mari G, Zotter A, Vermeulen W**.** DNA damage response. Cold Spring Harb
580 Perspect Bio. 2011; 3: a000745.
581 **28.** Waterman DP, Haber JE, Smolka MB. Checkpoint responses to DNA double-strand
582 breaks. Annu Rev Biochem. 2020; 89: 103-133.
583 **29.** Garcia JB, Rocha JP, Costa-Silva HM, Alves CL, Machado CR, Cruz AK. *Leishmania*
584 *major* and *Trypanosoma cruzi* present distinct DNA damage responses. Mol Biochem
585 Parasitol. 2016; 207: 23-32.

586 **30.** Machado-Silva A, Cerqueira PG, Grazielle-Silva V, Gadelha FR, Peloso Ede F,
587 Teixeira SM, et al. How *Trypanosoma cruzi* deals with oxidative stress: Antioxidant
588 defence and DNA repair pathways. Mutat Res Rev Mutat Res. 2015; 767: 8-22.
589 **31.** Gavrieli Y, Sherman Y, Ben-Sasson SA. Identification of programmed cell death *in*
590 *situ* via specific labeling of nuclear DNA fragmentation. J Cell Biol.1992; 119: 493-501.
591 **32.** Zhao W, Feng H, Sun W, Liu K, Lu JJ, Chen X. Tert-butyl hydroperoxide (t-BHP)
592 induced apoptosis and necroptosis in endothelial cells: Roles of NOX4 and
593 mitochondrion. Redox Biol. 2017; 11: 524-534.
594 **33.** Francisco AF, Jayawardhana S, Lewis MD, White KL, Shackleford DM, Chen G, et al.
595 Nitroheterocyclic drugs cure experimental *Trypanosoma cruzi* infections more
596 effectively in the chronic stage than in the acute stage. Sci Rep. 2016; 6: 35351.
597 **34.** Shields RK, Nguyen MH, Chen L, Press EG, Potoski BA, Marini RV, et al.
598 Pharmacokinetic and tissue distribution of benznidazole after oral administration in
599 mice. Antimicrob Agents Chemother. 2017; 61: e02410-16.
600 **35**. Seydel KB, Stanley SL. SCID mice and the study of parasitic disease. Clin Microbiol
601 Rev. 1996; 9: 126-134.
602 **36**. Magalhães LMD, Gollob KJ, Zingales B, Dutra WO. Pathogen diversity, immunity,
603 and the fate of infections: lessons learned from *Trypanosoma cruzi* human-host
604 interactions. Lancet Microbe 2022; 3: 711-722.
605 **37.** Bustamante JM, Sanchez-Valdez F, Padilla AM, White B, Wang W, Tarleton RL. A
606 modified drug regimen clears active and dormant trypanosomes in mouse models of
607 Chagas disease. Sci Transl Med. 2020; 12: eabb7656.
608 **38.** Resende BC, Oliveira ACS, Guañabens ACP, Repolês BM, Santana V, Hiraiwa PM,
609 et al. The influence of recombinational processes to induce dormancy in *Trypanosoma*
610 *cruzi.* Front Cell Infect Microbiol. 2020; 10: 5.
611 **39.** Zahoor A, Lafleur MV, Knight RC, Loman H, Edwards DI. DNA damage induced by
612 reduce nitroimidazole drugs. Biochem Pharmacol. 1987; 36: 3299-3304.

613 **40.** De Toranzo EGD, Castro JA, de Cazzulo BMF, Cazzulo JJ. Interaction of benznidazole
614 reactive metabolites with nuclear and kinetoplastic DNA, proteins and lipids from
615 *Trypanosoma cruzi*. Experientia 1998; 44: 880-881.
616 **41.** La-Scalea MA, Serrano SH, Ferreira EI, Brett AM. Voltammetric behavior of
617 benznidazole at a DNA-electrochemical biosensor. J Pharm Biomed Anal. 2002; 29:
618 561-568.
619 **42.** Francisco AF, Jayawardhana S, Olmo F, Lewis MD, Wilkinson SR, Taylor MC, et al.
620 Challenges in Chagas disease drug development. Molecules. 2020; 25: 2799.
621 **43.** Chatterjee N, Walker GC. Mechanisms of DNA damage, repair and mutagenesis.
622 Environ Mol Mutagen. 2017; 58: 235-263.
623 **44.** Machado-Silva A, Cerqueira PG, Grazielle-Silva V, Gadelha FR, Peloso Ede F,
624 Teixeira SM, et al. How *Trypanosoma cruzi* deals with oxidative stress: Antioxidant
625 defence and DNA repair pathways. Mutat Res Rev Mutat Res. 2016; 767: 8-22.
626 **45.** Martinez MZ, Olmo F, Taylor MC, Caudron F, Wilkinson SR. Dissecting the interstrand
627 crosslink DNA repair system of *Trypanosoma cruzi*. DNA Repair (Amst). 2023;
628 125: 103485.
629 **46.** Bustamante JM, White BE, Wilkerson GK, Hodo CL, Auckland LD, Wang W, et al.
630 Frequency variation and dose modification of benznidazole administration for the
631 treatment of *Trypanosoma cruzi* infection in mice, dogs, and nonhuman primates.
632 Antimicrob Agents Chemother. 2023; 67: e0013223.
633 **47.** Torrico F, Gascón J, Barreira F, Blum B, Almeida IC, Alonso-Vega C, et al. New
634 regimens of benznidazole monotherapy and in combination with fosravuconazole for
635 treatment of Chagas disease (BENDITA): a phase 2, double-blind, randomised trial.
636 Lancet Infect Dis. 2021; 21: 1129-1140.
637 **48.** Rao SPS, Gould MK, Noeske J, Saldivia M, Jumani RS, Ng PS, et al. Cyanotriazoles
638 are selective topoisomerase II poisons that rapidly cure trypanosome infections.
639 Science 2023; 380: 1349-1356.

640 **49.** Lewis MD, Francisco AF, Taylor MC, Kelly JM. A new experimental model for
641 assessing drug efficacy against *Trypanosoma cruzi* infection based on highly sensitive
642 *in vivo* imaging. J Biomolec Screen. 2015; 20: 36-43.
643 **50.** Lewis MD, Francisco AF, Taylor MC, Jayawardhana S, Kelly JM. Host and parasite
644 genetics shape a link between *Trypanosoma cruzi* infection dynamics and chronic
645 cardiomyopathy. Cell Microbiol. 2016; 18: 1429-1443.
646 **51.** Nakagawa A, Alt KV, Lillemoe KD, Castillo CF, Warshaw AL, Liss AS. A method for
647 fixing and paraffin embedding tissue to retain the natural fluorescence of reporter
648 proteins. Biotechniques 2015; 59: 153-155.
649
650
651
652
653
654
655
656
657
658
659
660
661
662
663
664
665
666

667 **Figure 1. Assessing benznidazole treatment conditions to optimise the generation of *T.***
668 ***cruzi* persisters.** (a) MA104 cells were infected with *T. cruzi* CL Luc::mNeon [22] in 24-well
669 plates containing 13-mm diameter glass coverslips, incubated for 3 days, and then treated
670 with benznidazole for 8 days at a range of concentrations (5-30 μM) (Materials and Methods).
671 Each day, selected cultures were exposed to 10 μM EdU for 6 hours, fixed on coverslips,
672 developed and scanned by fluorescence microscopy. The data are presented as % infected
673 host cells containing at least one EdU+ve amastigote. (b) Upper image; an infected cell prior
674 to drug exposure, with parasites that are in S-phase during the exposure period shown in red
675 (EdU incorporation). DAPI staining (blue) identifies host cell nuclei and amastigotes, which are
676 recognisable by their distinctive disc-like kinetoplast genome (orange arrow). Lower image; an
677 infected cell after 8 days exposure to 10 μM benznidazole. The two amastigotes highlighted
678 by arrows did not undergo DNA replication during the period of EdU exposure. The adjacent
679 red stained host cell nucleus serves as a positive control for EdU labelling. White scale bars
680 = 10 μm. (c) Infected cell monolayers in 24-well plates (as above) were treated with 20 μM
681 benznidazole. On the days indicated, a coverslip was fixed and the amastigote content of
682 randomly selected infected cells recorded. By day 5, all imaged infected cells contained a
683 single amastigote. Average intracellular burden indicated by red line. (d) Infected monolayers
684 in 24-well plates were treated with benznidazole for 8 days at the concentrations indicated.
685 After washing, cultures were maintained in MEM for 32 days and monitored for the appearance
686 of extracellular differentiated trypomastigotes. This assay period (a total of ~50 days) is the
687 limit attainable with monolayers of MA104 cells.
688
689
690 **Figure 2. Isolation of intracellular *T. cruzi* persisters by live cell sorting following *in vitro***
691 **benznidazole treatment.** (a) Experimental outline. Cultures of MA104 cells were infected with
692 *T. cruzi* CL Luc::mNeon parasites. After 72 hours, they were treated with 20 μM benznidazole
693 for a further 8 days. Cellular suspensions were then generated for analysis by live cell sorting
694 (Materials and Methods). (b) Live fluorescence images of a cellular suspension showing DNA

695 (Hoechst staining, blue), non-viable cells (propidium iodide (PI) staining, red) and parasite-
696 infected cells (green fluorescence). In the merged image (right), the white arrow indicates a *T.*
697 *cruzi* infected MA104 cell. Yellow scale bar = 50 μm. (c) Fractionation of infected cell
698 suspension, following PI staining, using an Aria BD Cell Sorter. The small percentage of non-
699 viable cells can be separated on the basis of acquired PI fluorescence. (d) Fractionation of
700 live host cells into infected (within red circle) and non-infected sub-populations based on the
701 green fluorescence of parasite persisters. 0, background fluorescence; G, lowest green
702 fluorescence gating. (e) Image of an infected cell subpopulation suspension post-sorting. The
703 number of parasites in each cell is indicated (1 or 2). (f) Sorted infected cells 18 hours post-
704 plating (Materials and Methods). DNA, (blue); amastigotes, (green).
705
706
707 **Figure 3. Assessing the replicative status of persister parasites *in vitro* following**
708 **benznidazole treatment.** MA104 cells were infected with *T. cruzi* CL Luc::mNeon in 24-well
709 plates as indicated, and after 3 days growth, they were treated with 20 μM benznidazole for 8
710 days. When benznidazole was removed, the cells were maintained in complete MEM and
711 monitored by fluorescence microscopy. To identify parasites undergoing DNA replication,
712 cultures were exposed to 10 μM EdU for 6 hours and the coverslips processed for analysis
713 using a Zeiss LSM880 confocal microscope (Materials and Methods). (a) Amastigote numbers
714 in infected cells immediately after drug removal, and at day 11 post-treatment. The number of
715 EdU+ve parasites is shown in red. (b) Timeline of an independent experiment in which the
716 number of EdU+ve amastigotes was assessed periodically after the cessation of treatment.
717 (c) A pre-treatment parasite nest in which ~50% of the amastigotes are in S-phase during the
718 period of EdU exposure (red). DAPI staining (blue) identifies host cell nuclei (large) and the
719 parasite kinetoplast DNA (small, intense blue discs). (d) At 6 days post-wash, amastigotes
720 (green) are in a non-replicative state. An MA104 cell in S-phase is identified by nuclear EdU
721 staining (red). (e) Images showing parasites that have re-entered the cell cycle (day 11) and
722 are undergoing asynchronous DNA replication [24]. White scale bars = 10 μm.

723

724

725 **Figure 4. Fragmentation of *T. cruzi* DNA following benznidazole treatment.** (a)
726 Experimental outline. MA104 cells were infected with *T. cruzi* CL Luc::mNeon in 24-well plates.
727 They were treated with either benznidazole (BZ) (200 μM) for 24 hours, or tert-butyl
728 hydroperoxide (TBHP) (50 μM) for 3 days. Post-fixation, as a control group, untreated cells
729 were treated with DNase. TUNEL assays were then performed and cells imaged using a Nikon
730 Ti-2 E inverted microscope (Materials and Methods). (b) Representative images showing
731 infected cells following each of the treatments. Parasites (green fluorescence), DNA (blue,
732 DAPI), TUNEL (red). The enlarged inset (left) highlights replicating kinetoplast DNA (kDNA).
733 The white arrows in the non-treated images show the location of a highly infected cell in which
734 all the parasites have differentiated into TUNEL-negative non-replicating trypomastigotes.
735 White scale bars = 10 μm.

736

737

738 **Figure 5. Monitoring the tissue-specific impact of non-curative benznidazole treatment**
739 **by bioluminescence imaging**. (a) Representative *in vivo* images of *T. cruzi* infected BALB/c
740 mice after once daily oral treatment with 25 mg/kg benznidazole for 5 days (Materials and
741 Methods). Treatment was initiated in the acute stage either 9 (pre-peak) or 14 (peak) days
742 post-infection (dpi). The percentage drop in whole-body bioluminescence is indicated (n=6).
743 (b) Schematic showing the arrangement of tissues, organs and carcass used for *ex vivo*
744 imaging. (c) *Ex vivo* images of non-treated and treated infected mice. The heat-map for both
745 *ex vivo* and *in vivo* imaging is on a log10 scale and indicates the intensity of bioluminescence
746 from low (blue) to high (red) with minimum and maximum radiance values as indicated. (d)
747 Fluorescent detection of parasites in the bladder and cardiac muscle of non-treated and
748 treated mice during the acute stage of infection, using a Zeiss LSM880 confocal laser scanning
749 microscope. DNA (red, DAPI); parasites (green fluorescence; yellow, if on a red background).
750 White scale bars = 20 μm. Lower images show expanded view of single amastigote infections.

751

752

753 **Figure 6. In benznidazole treated mice, the majority of cells that remain infected contain**
754 **only a single parasite.** BALB/c mice in the pre-peak (9 dpi) and peak (14 dpi) stages of
755 infection were treated once daily with 25 mg/kg benznidazole for 5 days (as in Figure 5). Serial
756 sections (10 μm) from a range of tissues were prepared and examined in 3-dimensions by z-
757 stacking to determine the precise number of amastigotes in each infected cell (Materials and
758 Methods) (see also S1 Video). (a) Illustrative 0.7 μm serial images across a section of cardiac
759 tissue from a non-treated mouse. Amastigotes (green); DNA (blue, DAPI). Parasite numbers
760 can be determined with precision by counting the distinctive intensely stained kinetoplast
761 (mitochondrial) DNA that co-localises with green fluorescence across serial sections. White
762 scale bar = 5 μm. (b) Parasite numbers per infected cell determined by exhaustive screening
763 of multiple sections obtained from a range of tissues from treated (orange bars) and non-
764 treated (blue bars) mice.

765

766

767 **Figure 7. Parasites that persist in mouse cardiac tissue after benznidazole treatment**
768 **are in a non-replicative state.** CB17 SCID mice were infected with *T. cruzi* and 10 days post-
769 infection they were treated once daily with 25 mg/kg benznidazole for 5 days. EdU labelling
770 was then carried out as described previously (Materials and Methods). Mice were euthanised
771 (16 dpi), and cardiac sections prepared and imaged using a Nikon Ti-2 E inverted microscope
772 (9 mice per group, 3 randomly selected sections from each mouse) (a) Infection burden per
773 infected cardiac cell (nest), with the number of EdU+ve/-ve parasites indicated (see also S3
774 Figure). (b) Images showing an infected cardiomyocyte from a non-treated mouse that
775 contains both replicating and non-replicating amastigotes. The inset shows an example of a
776 single serial cross section derived by 3-dimensional confocal laser scanning microscopy (z-
777 stacking), which was used to determine the precise number of amastigotes in the infected cell
778 (white arrow indicates intensely stained kinetoplast DNA) (see S1 Video for 3-dimensional

image of this infected cell). DNA (blue, DAPI); EdU+ve amastigotes (red); parasites (green fluorescence). White scale bar = 10 μm. (c) Images of infected cardiomyocytes from benznidazole-treated mice. None of the amastigotes detected were EdU+ve. A purple arrow indicates two host cells that were in S-phase during the period of EdU exposure (upper image). White scale bars = 20 μM. The insets (right) show enlarged images of DAPI stained host cell nuclei and single infecting amastigotes (green). Full 3-dimensional images of parasites that persist after benznidazole treatment are shown in S2 and S3 Videos.

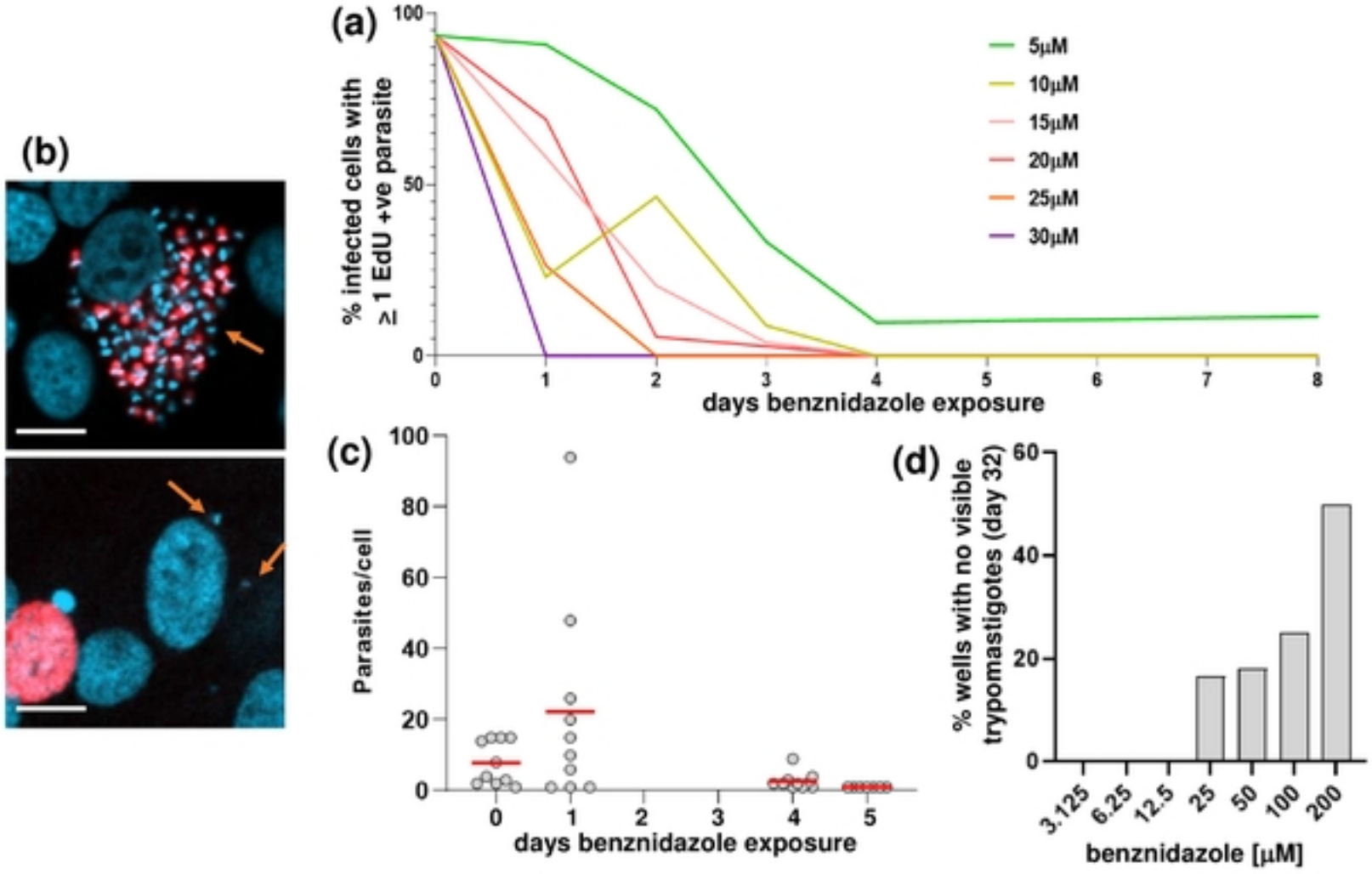
(a)
% infected cells with ≥1 EdU +ve parasite
100
50
0
0
1
2
3
4
5
6
7
8
days benznidazole exposure
5μM
10μM
15μM
20μM
25μM
30μM
(b)
(c)
Parasites/cell
100
80
60
40
20
0
0
1
2
3
4
5
days benznidazole exposure
(d)
% wells with no visible trypomastigotes (day 32)
60
40
20
0
3.125
6.25
12.5
25
50
100
200
benznidazole [μM]

Fig. 1

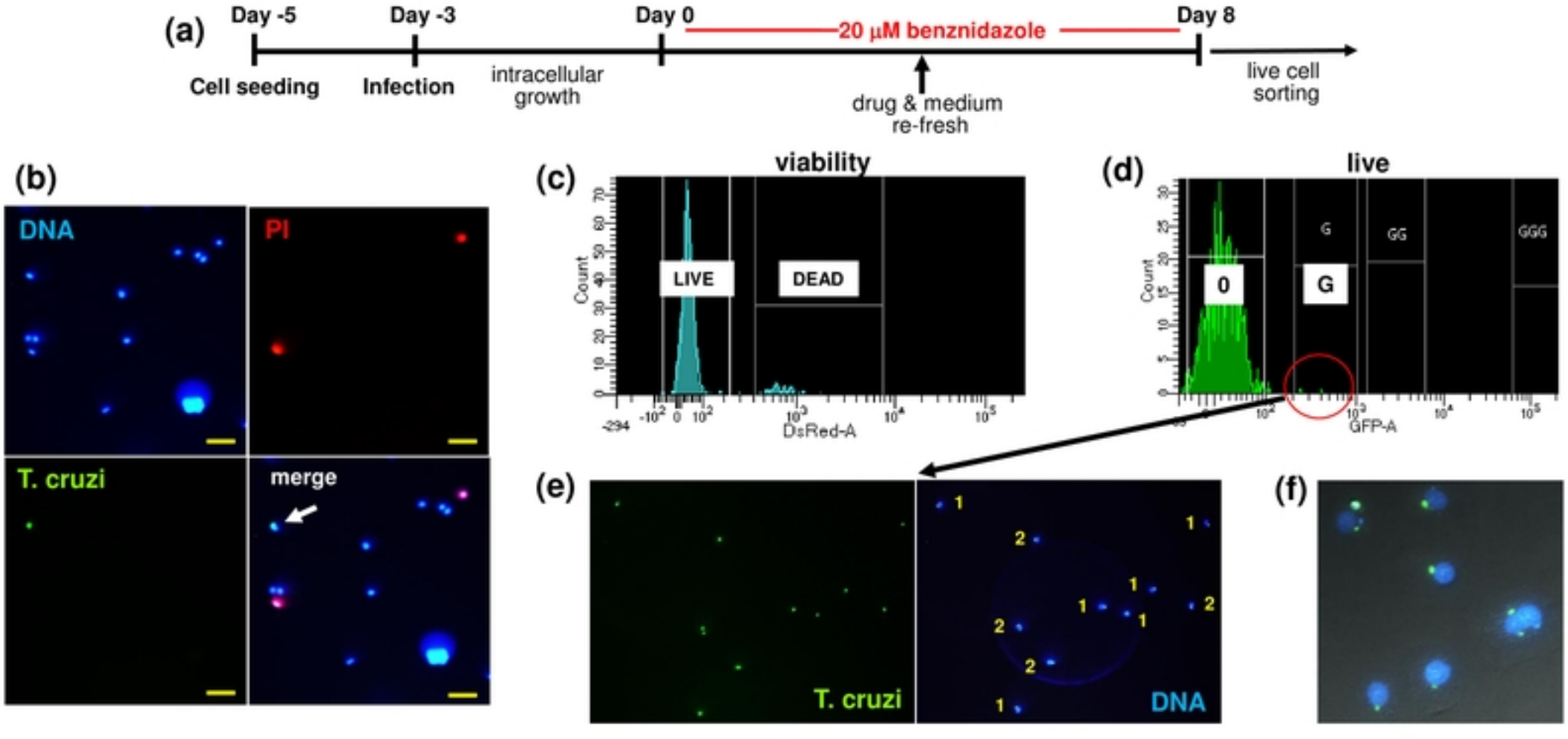
(a)
Day -5
Day -3
Day 0
20 µM benznidazole
Day 8
Cell seeding
Infection
intracellular growth
drug & medium re-fresh
live cell sorting
(b)
DNA
PI
T. cruzi
merge
(c)
viability
LIVE
DEAD
Count
DsRed-A
(d)
live
0
G
GG
GGG
Count
GFP-A
(e)
T. cruzi
DNA
(f)

Fig. 2

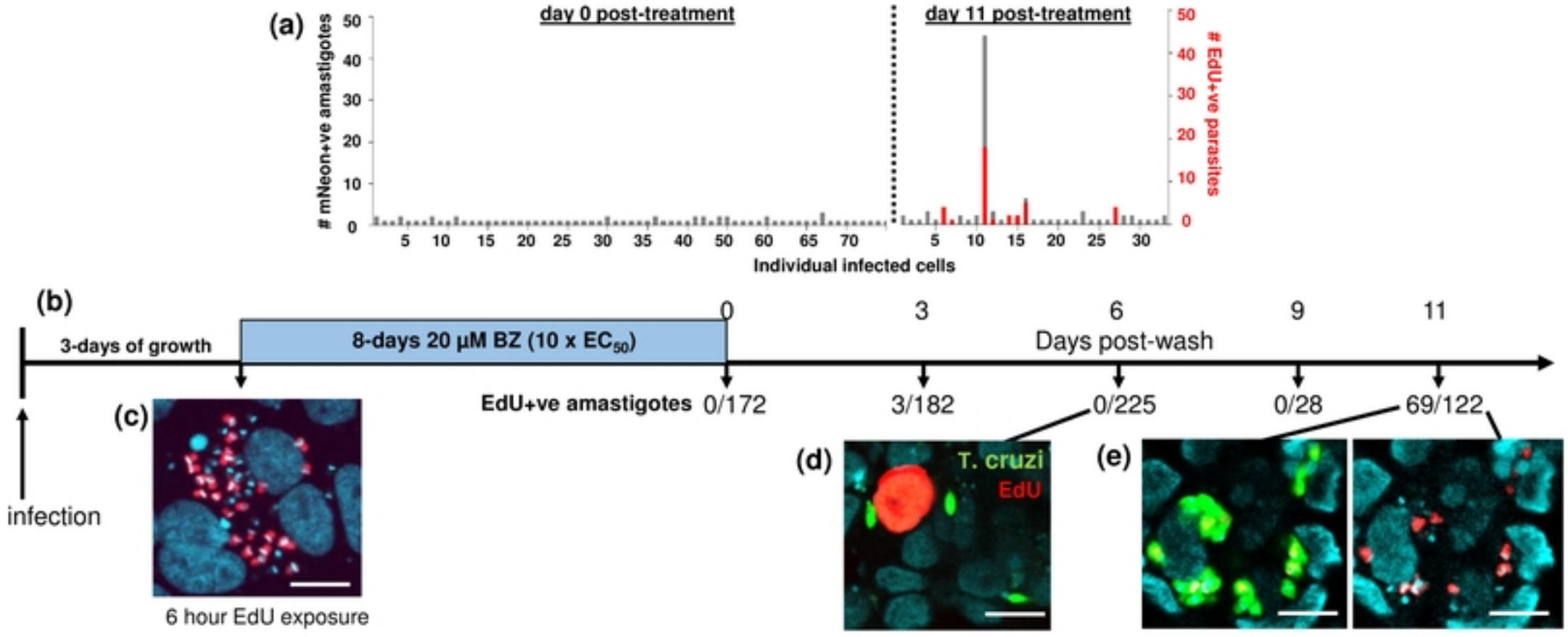
(a)
day 0 post-treatment
day 11 post-treatment
mNeon+ve amastigotes
EdU+ve parasites
Individual infected cells
(b)
3-days of growth
8-days 20 µM BZ (10 x EC50)
Days post-wash
0
3
6
9
11
EdU+ve amastigotes
0/172
3/182
0/225
0/28
69/122
infection
(c)
6 hour EdU exposure
(d)
T. cruzi
EdU
(e)

Fig. 3

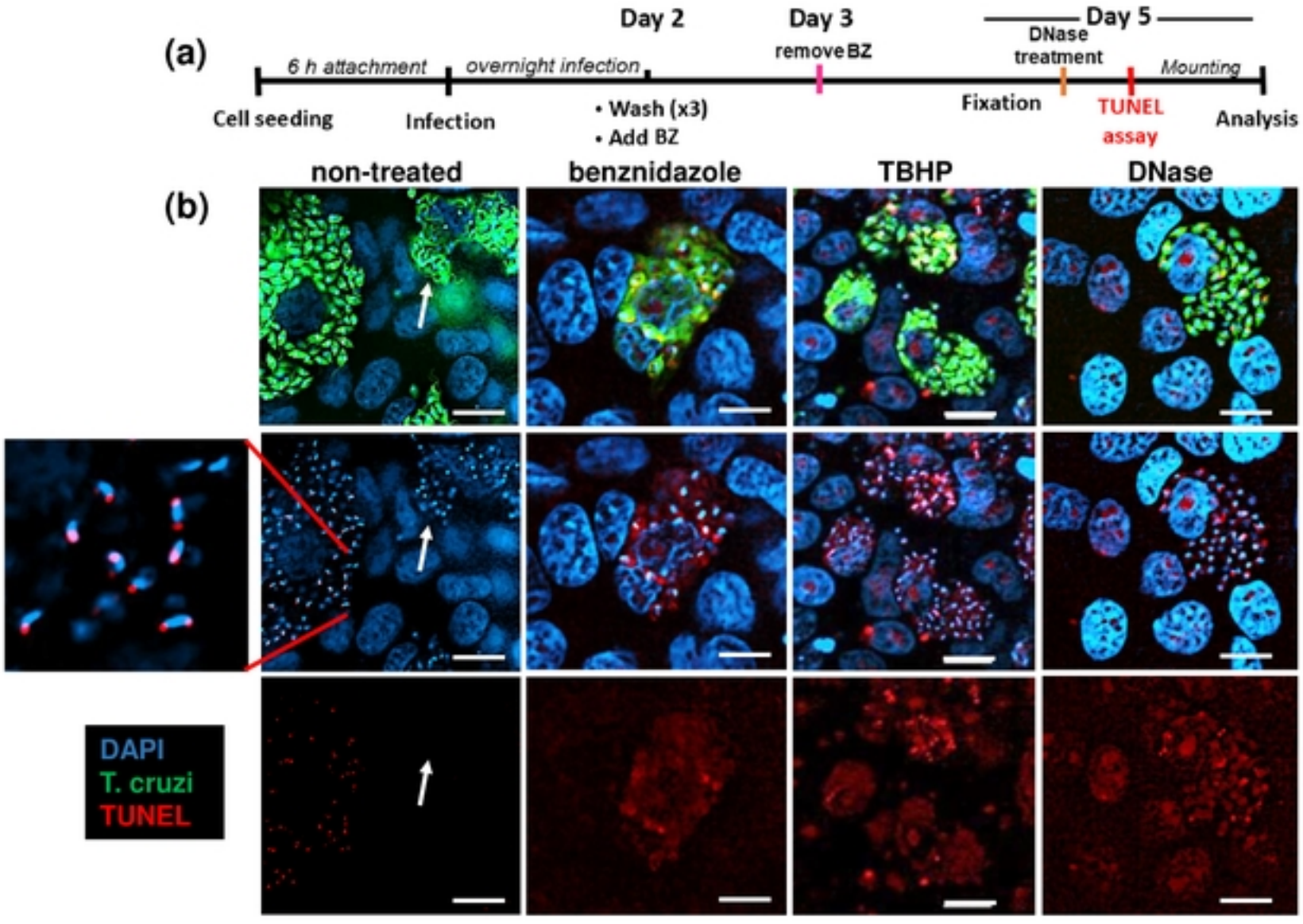
(a)
Day 2
Day 3
Day 5
6 h attachment
overnight infection
remove BZ
DNase treatment
Mounting
Cell seeding
Infection
• Wash (x3)
• Add BZ
Fixation
TUNEL assay
Analysis
(b)
non-treated
benznidazole
TBHP
DNase
DAPI
T. cruzi
TUNEL

Fig. 4

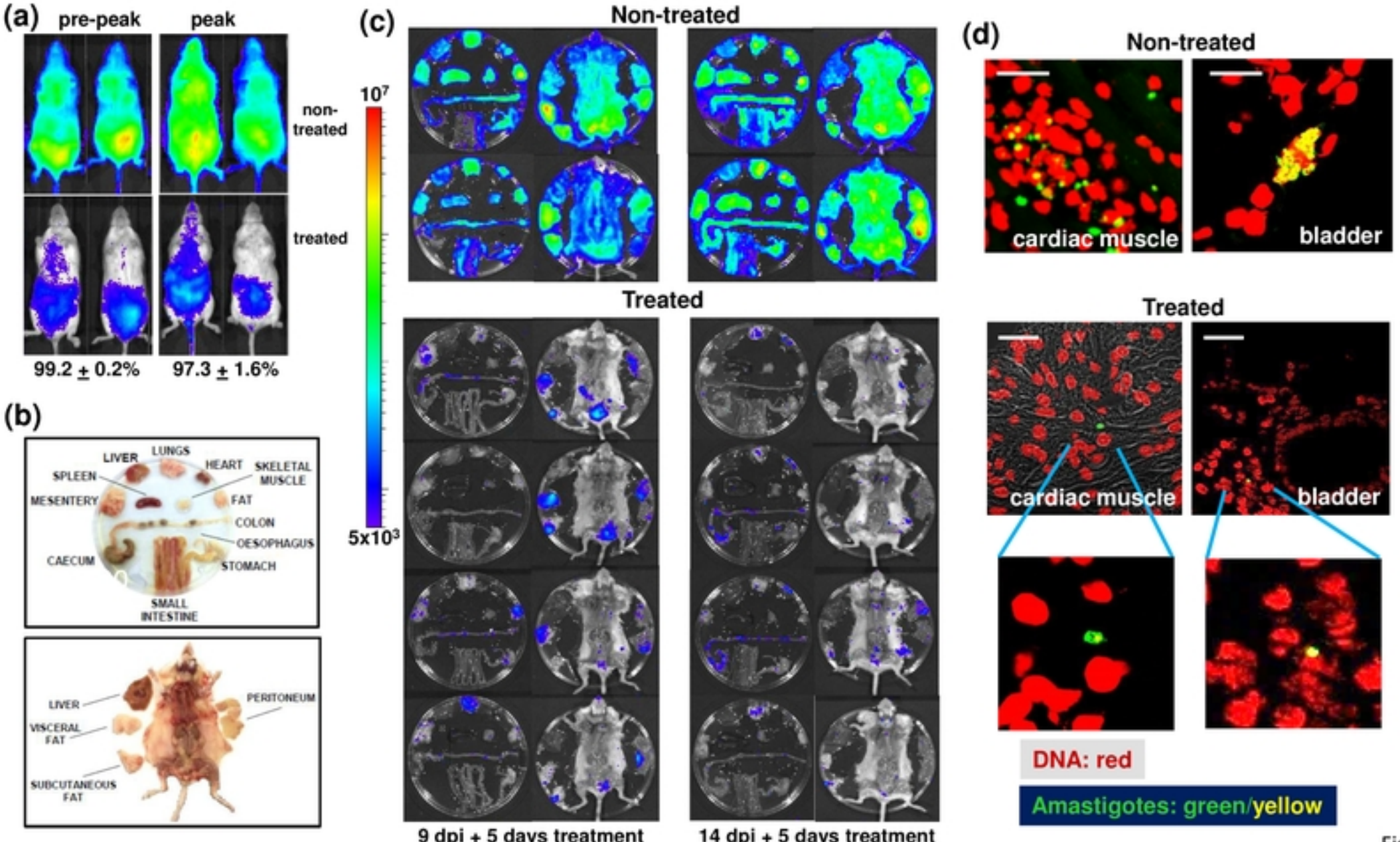
(a)
pre-peak
peak
non-treated
treated
99.2 ± 0.2%
97.3 ± 1.6%
(b)
LIVER
LUNGS
HEART
SKELETAL MUSCLE
SPLEEN
MESENTERY
FAT
COLON
OESOPHAGUS
CAECUM
STOMACH
SMALL INTESTINE
LIVER
PERITONEUM
VISCERAL FAT
SUBCUTANEOUS FAT
(c)
Non-treated
Treated
10^7
$5x10^3$
9 dpi + 5 days treatment
14 dpi + 5 days treatment
(d)
Non-treated
cardiac muscle
bladder
Treated
cardiac muscle
bladder
DNA: red
Amastigotes: green/yellow

Fig. 5

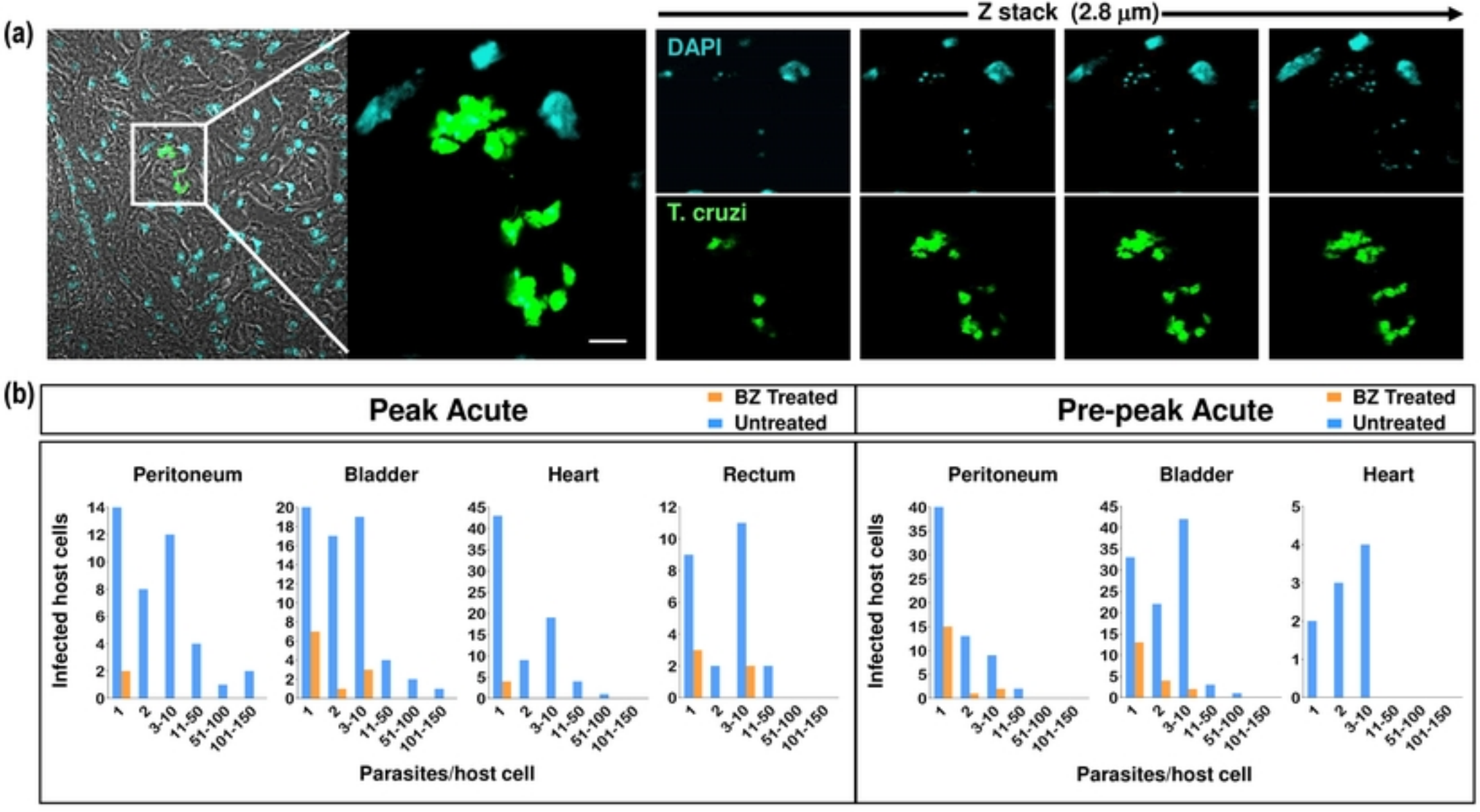
(a)
Z stack (2.8 µm)
DAPI
T. cruzi
(b)
Peak Acute
BZ Treated
Untreated
Pre-peak Acute
BZ Treated
Untreated
Peritoneum
Bladder
Heart
Rectum
Peritoneum
Bladder
Heart
Infected host cells
Parasites/host cell
1
2
3-10
11-50
51-100
101-150

Fig. 6

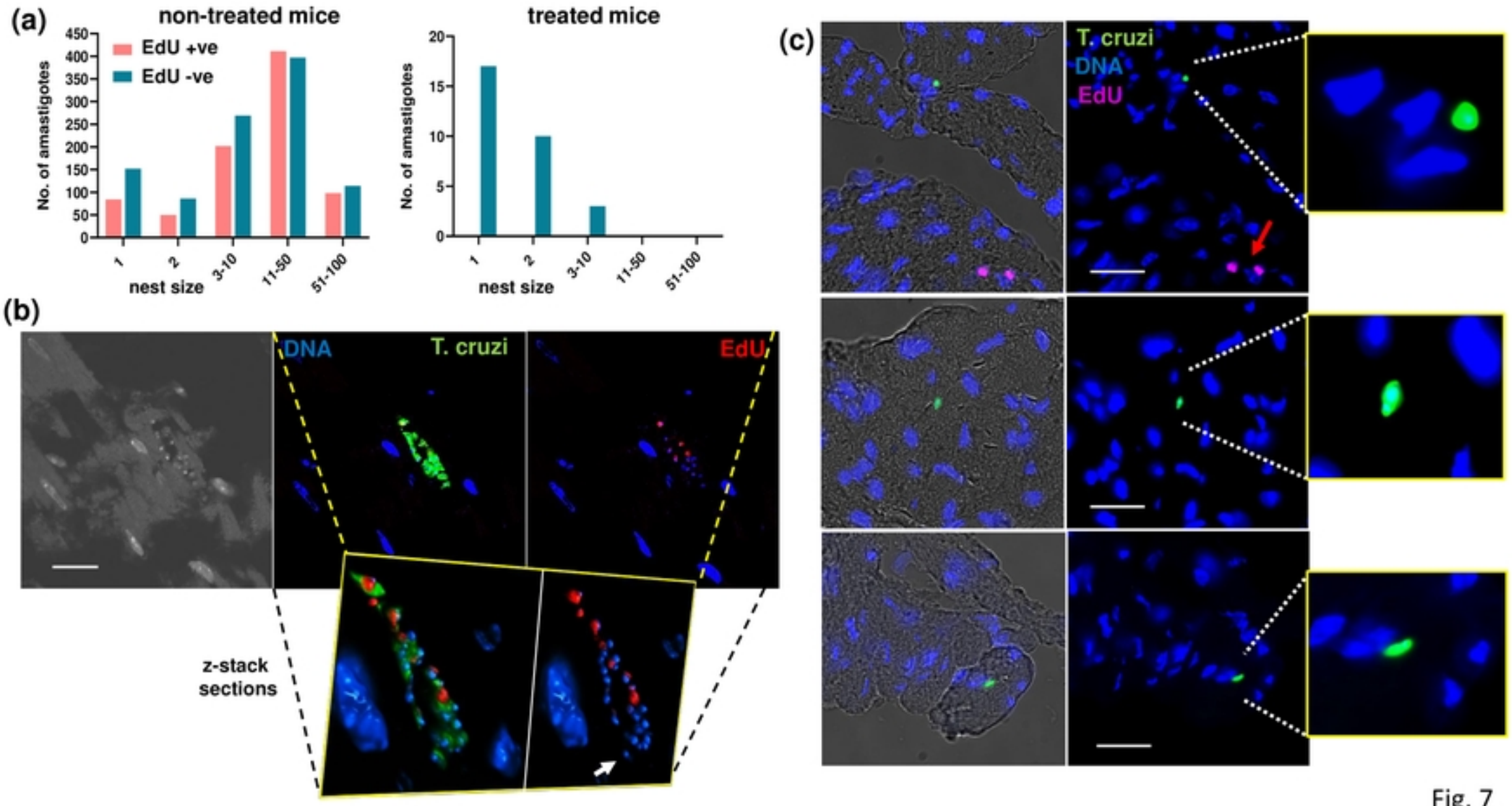
(a)
non-treated mice
EdU +ve
EdU -ve
No. of amastigotes
nest size
1
2
3-10
11-50
51-100
treated mice
(b)
DNA
T. cruzi
EdU
z-stack sections
(c)
T. cruzi
DNA
EdU

Fig. 7